Transactions in GIS, 2010, 14(5): 615–630

Research Article

An Adaptive Method of High Accuracy Surface Modeling and Its Application to Simulating Elevation Surfaces

Tian-Xiang Yue
Institute of Geographical Sciences and Natural Resources Research, Beijing, China and Ecological Complexity and Modeling Laboratory University of California, Riverside

Chuan-Fa Chen
School of Civil Engineering, Shandong Jianzhu University

Bai-Lian Li
Ecological Complexity and Modeling Laboratory, University of California, Riverside

Abstract
An adaptive method is employed to speed up computation of high accuracy surface modeling (HASM), for which an error indicator and an error estimator are developed. Root mean-square error (RMSE) is used as the error estimator that is formulated as a function of gully density and grid cell size. The error indicator is developed on the basis of error surfaces for different spatial resolutions, which are interpolated in terms of the absolute errors calculated at sampled points while paying attention to the landform characteristics. The error surfaces indicate the magnitude and distribution of errors in each step of adaptive refinement and make spatial changes to the errors in the simulation process visualized. The adaptive method of high accuracy surface modeling (HASM-AM) is applied to simulating elevation surface of the Dong-Zhi tableland with 27.24 million pixels at a spatial resolution of 10 m × 10 m. Test results show that HASM-AM has greatly speeded up computation by avoiding unnecessary calculations and saving memory. In addition, HASM-AM improves simulation accuracy.

Address for correspondence: Tian-Xiang Yue, Institute of Geographical Sciences and Natural Resources Research, 100101 Beijing, China. E-mail: yue@lreis.ac.cn

doi: 10.1111/j.1467-9671.2010.01213.x

1 Introduction

Elevation is the z-value in the third dimension to complement the x-value and y-value representing location in a two-dimensional space (Atkinson 2002). Elevation is an inexpensive and intensively sampled variable, and one of the most needed. Elevation surfaces (ESs) are a fundamental input for various applications such as spatial analyses of climate change, population distribution and ecosystem changes as well as hydrological modeling and global circulation modeling (Kidner et al. 2000; Schneider 2001; Yue et al. 2003, 2005, 2006). Accuracy of ESs is of crucial importance because errors will propagate and impact spatial analyses (Leigh et al. 2009).

An ES, even one of the highest quality, is an approximation to the continuous real-world surface. ES errors include sampling errors, the errors introduced from data-capturing equipment, errors introduced in the transformation of control points, errors from the mathematical model for constructing the surface, the errors propagated from the data source, representation errors, and errors caused by grid resolution and orientation (Zhou and Liu 2002). The ES errors can be propagated through the simulation process and become manifest in the final products (Huang and Lees 2005). Although there are many types and sources of error and uncertainty in geographical data and their processing, the problem is not simply technical (Unwin 1995) and it arises from an evident drawback of GIS, which lacks a complete theoretical foundation for surface modeling.

To find a solution for the error problem that had long troubled surface modeling, a method for high accuracy surface modeling (HASM) was developed (Yue et al. 2007, 2008). Both numerical tests and real-world studies showed that accuracy of HASM was much higher than the classical methods such as inverse distance weighting (IDW), Kriging and splines (Yue 2010, Yue and Song 2008). However, computational speed of HASM was too slow to be widely applied. Thus, HASM is combined with an adaptive method to speed up computation in this article.

1.1 Adaptive Method

In most numerical procedures for solving partial differential equations, the problem is first discretized by choosing algebraic equations on a finite-dimension approximation space and then a numerical process is devised to solve this huge system of discrete equations. The discretization process, which was unable to predict the proper resolution and the proper order of approximation at each location, produced a grid that was too fine. The algebraic system thus became unnecessarily large in size, while accuracy usually remained rather low (Brandt 1977). The aim of adaptive methods is the generation of a grid that is adapted to the problem such that a given error criterion is fulfilled by the solution on this grid. An optimal grid should be as coarse as possible while meeting the criterion in order to save computing time and memory requirements (Schmidt and Siebert 2005). For stationary issues, a grid is almost optimal when the local errors are approximately equal for all elements. Therefore elements where the error is large will be marked for refinement, while elements with a small estimated error are left unchanged or are marked for coarsening.

Adaptive procedures for the numerical solution of differential equations started in the late 1950s. Birchfield (1960) found that reduction of truncation error by the use of a smaller grid resulted in improved forecasts of hurricane movement trajectories, in which 150 km × 150 km grid cells only covered the neighborhood of the vortex and the remaining part of the region was covered by 300 km × 300 km grid cells. Morrison (1962) stated that in the integration of a system of ordinary differential equations, the simplest approach was to use a fixed step size, but over some parts of the range of integration it was generally possible to take a larger step size without seriously affecting the local truncation error. Harrison (1973) suggested that the domain to be resolved with the highest resolution could be kept to a minimum in order to reduce the computer space and time requirements significantly; utilizing a gradual reduction in grid scale would essentially allow one to focus on a region of interest with a very fine grid, while still maintaining relatively coarse resolution in the surrounding area. Ley and Elsberry (1976) indicated that it seemed natural to consider a multiple-nested grid arrangement rather than maintaining the same grid size throughout the domain if very fine resolution was only required near the center.

1.2 HASM

Slope, aspect and curvature are significant variables of surface analysis (Evans 1980). Thus, a method for surface modelling of cirques was constructed (Yue and Ai 1990) and then developed to detect changes of earth surface systems (Yue et al. 2002). However, curvature, slope and intercept uniquely define a curve according to the fundamental theorem of curves (Okubo 1987). A surface is uniquely defined by the first and the second fundamental coefficients according to the fundamental theorem of surfaces (Toponogov 2006). High accuracy surface modeling (HASM) was thus developed in terms of the fundamental theorem of surfaces (Yue 2010, Yue et al. 2007).

If a surface is a graph of a function $z = \mathrm{u}(x,y)$ or $r = (x,y,u(x,y))$, the basic theoretical equations of HASM could be formulated as:

$$\mathrm{u}_{xx} = \Gamma_{11}^{1} \cdot \mathrm{u}_x + \Gamma_{11}^{2} \cdot \mathrm{u}_y + L \cdot (E \cdot G - F^2)^{-\frac{1}{2}} \tag{1}$$

$$\mathrm{u}_{yy} = \Gamma_{22}^{1} \cdot \mathrm{u}_x + \Gamma_{22}^{2} \cdot \mathrm{u}_y + N(E \cdot G - F^2)^{-\frac{1}{2}} \tag{2}$$

where superscripts of Γ_{11}^{1}, Γ_{11}^{2}, Γ_{22}^{1} and Γ_{22}^{2} denote labels; other superscripts denote powers; $E = 1 + \mathrm{u}_x^2$; $F = \mathrm{u}_x\mathrm{u}_y$; $G = 1 + \mathrm{u}_y^2$; $L = \dfrac{\mathrm{u}_{xx}}{\sqrt{1 + \mathrm{u}_x^2 + \mathrm{u}_y^2}}$; $N = \dfrac{\mathrm{u}_{yy}}{\sqrt{1 + \mathrm{u}_x^2 + \mathrm{u}_y^2}}$; $\Gamma_{11}^{1} = \frac{1}{2}(GE_x - 2FF_x + FE_y)(EG - F^2)^{-1}$; $\Gamma_{11}^{2} = \frac{1}{2}(2EF_x - EE_y - FE_x)(EG - F^2)^{-1}$; $\Gamma_{22}^{1} = \frac{1}{2}(2GF_y - GG_x - FG_y)(EG - F^2)^{-1}$; $\Gamma_{22}^{2} = \frac{1}{2}(EG_y - 2FF_y + FG_x)(EG - F^2)^{-1}$; $EG - F^2 = E + G - 1 = u_x^2 + u_y^2 + 1$.

The first and second fundamental coefficients, E, F, G, L and N must be firstly calculated in terms of sampled values when u is simulated. If $\{\overline{u}_{ij}\}$ are the sampled values of u at sampling points $\{(x_i,y_i)\}$ and $\{\tilde{u}_{i,j}\}$ are interpolations in terms of the sampled

values $\{\overline{u}_{ij}\}$. Let $u_{ij}^0 = \tilde{u}_{ij}$ and h represents simulation step length, then the $(n+1)$th iteration of HASM could be formulated as:

$$\frac{u_{i+1,j}^{(n+1)} - 2u_{i,j}^{(n+1)} + u_{i-1,j}^{(n+1)}}{h^2} = \left(\Gamma_{11}^1\right)_{i,j}^{(n)} \frac{u_{i+1,j}^{(n)} - u_{i-1,j}^{(n)}}{2h} + \left(\Gamma_{11}^2\right)_{i,j}^{(n)} \frac{u_{i,j+1}^{(n)} - u_{i,j-1}^{(n)}}{2h} + \frac{L_{i,j}^{(n)}}{\sqrt{E_{i,j}^{(n)} + G_{i,j}^{(n)} - 1}} \tag{3}$$

$$\frac{u_{i,j+1}^{(n+1)} - 2u_{i,j}^{(n+1)} + u_{i,j-1}^{(n+1)}}{h^2} = \left(\Gamma_{22}^1\right)_{i,j}^{(n)} \frac{u_{i+1,j}^{(n)} - u_{i-1,j}^{(n)}}{2h} + \left(\Gamma_{22}^2\right)_{i,j}^{(n)} \frac{u_{i,j+1}^{(n)} - u_{i,j-1}^{(n)}}{2h} + \frac{N_{i,j}^{(n)}}{\sqrt{E_{i,j}^{(n)} + G_{i,j}^{(n)} - 1}} \tag{4}$$

where $n \geq 0$; $u_{0,j}^{(0)}$, $u_{i,0}^{(0)}$, $u_{M+1,j}^{(0)}$ and $u_{i,M+1}^{(0)}$ are boundary conditions.

If the computational domain is normalized to $[0,1] \times [0,1]$, the basic equations can be expressed as:

$$A_1 U^{(n+1)} = B_1^{(n)} \tag{5}$$

$$A_2 U^{(n+1)} = B_2^{(n)} \tag{6}$$

where $U^{(n+1)} = \left(u_{1,1}^{(n+1)}, \cdots, u_{1,M}^{(n+1)}, u_{2,1}^{(n+1)}, \cdots, u_{2,M}^{(n+1)}, \cdots\cdots, u_{M-1,1}^{(n+1)}, \cdots, u_{M-1,M}^{(n+1)}, u_{M,1}^{(n+1)}, \cdots, u_{M,M}^{(n+1)}\right)^T$; $M+2$ is the lattice number in direction x or direction y; $h = \frac{1}{M+1}$; A_1 and $B_1^{(n)}$ are respectively the matrix of the left-hand item and the vector of the right-hand item of equation (3); A_2 and $B_2^{(n)}$ are respectively the left-hand-item matrix and right-hand-item vector of equation (4).

If $Z = \begin{bmatrix} A_1 \\ A_2 \end{bmatrix}$ and $Q^{(n)} = \begin{bmatrix} B_1^{(n)} \\ B_2^{(n)} \end{bmatrix}$, the following least squares algorithm can be developed to make the simulated values equal to sampled values at the sampling points:

$$\begin{cases} \min \left\| ZU^{(n+1)} - Q^{(n)} \right\|_2 \\ s.t. \quad CU^{(n+1)} = D \end{cases} \tag{7}$$

where $C(k,(i-1)\cdot M + j) = 1$ and $D(k) = \overline{u}_{i,j}$, which means that the sampled value is $\overline{u}_{i,j}$ at the kth sampling point (x_i, y_j).

For sufficiently large λ, the algorithm (7) can be transferred into an unconstrained least squares approximation:

$$\min_F \left\| \begin{bmatrix} Z \\ \lambda C \end{bmatrix} U^{(n+1)} - \begin{bmatrix} Q^{(n)} \\ \lambda D \end{bmatrix} \right\|_2 \tag{8}$$

or

$$\begin{bmatrix} Z^T & \lambda C^T \end{bmatrix} \begin{bmatrix} Z \\ \lambda C \end{bmatrix} U^{(n+1)} = \begin{bmatrix} Z^T & \lambda C^T \end{bmatrix} \begin{bmatrix} Q^{(n)} \\ \lambda D \end{bmatrix} \tag{9}$$

The parameter λ is the weight of the sampling points and determines the contribution of the sampling points to the simulated surface. λ could be a real number, which means all

sampling points have the same weight, or a sector, which means every sampling point has its own weight. The area affected by a sampling point in a complex region is smaller than in a flat region. Therefore, a smaller value of λ is selected in a complex region and a bigger value of λ is selected in a flat region.

We formulate $A_h = [Z^T \quad \lambda C^T]\begin{bmatrix} Z \\ \lambda C \end{bmatrix}$ and $B_h^{(n)} = [Z^T \quad \lambda C^T]\begin{bmatrix} Q^{(n)} \\ \lambda D \end{bmatrix}$ under consideration of the simulation step length (or grid cell size) h. Then, formulation (9) can be expressed as (Yue and Song 2008):

$$A_h U^{(n+1)} = B_h^{(n)} \tag{10}$$

2 Elevation Surface Simulation of the Dong-Zhi Tableland

2.1 Data Acquisition

Dongzhi tableland with its elevation of 1,350 m on average is located from 35°28′ to 35°40′*N* and from 107°39′ to 108°05′*E*. The total area is 2,778 km^2 and the relatively flat land covers 910 km^2. The Dongzhi tableland was formed 2 million years ago. Scholars mostly believe that loess plateau surfaces came into being after synthetic geological effects for several million years under the influence of wind on loess. The Dongzhi tableland is acclaimed as "the first loess tableland" because it has the biggest flat land and the deepest soil depth in China's loess plateau. The original Dongzhi tableland, which was relatively homogeneous, has become fragmented and crisscrossed with gullies because of vegetation reduction and soil erosion. The eroded area is 2,724 km^2, accounting for 98.1% of the total area (Figure 1 and Table 1). The serious soil erosion leads to the rapid shrinkage of the tableland surface. According to historic records, the Dongzhi tableland was 110 km in length and 32 km in width during the period 618 to 917. However, the widest area of the Dongzhi tableland is 18 km and the narrowest area is only 0.05 km although its length is almost the same as before.

Parts of 197 relief maps that together cover the Dongzhi tableland were scanned and digitized, among which 60 pieces are on the scale of 1/5,000 and 137 pieces on the scale of 1/10,000. The relief maps include contour lines and 6,692 sampled heights of high accuracy scattered over the Dongzhi tableland. Errors created in the scanning process are corrected by comparing every piece of the original contour map with the sampled heights. Then all the scanned pieces of the contour maps are combined into a whole by jointing ends of contour lines in the different pieces. The Gauss-Krueger projection, in which each zone is 3° of longitude in width, is adopted to transform Beijing geographical coordinates established in 1954 into rectangular Cartesian coordinates for easier calculation and the Dongzhi tableland is projected to the 36th zone. The Huang-Hai Elevation System, established in 1956, is used as the elevation datum. After the transformation of the coordinate system, the contour lines are transformed into scattered points and the sampled heights high accuracy are used to test the simulated elevation surface and to create error surfaces in terms of absolute error.

Figure 1 Vector map of Dong-Zhi tableland generated by digitizing parts of 197 relief maps

Table 1 Terrain parameters of the Dongzhi tableland

Terrain parameters	Relatively flat area	Eroded tableland	Terrace	Bridge	Hill	Gully
Standard deviation of elevation (m)	20.9	43.0	64.4	74.3	60.4	69.0
Mean elevation (m)	1,371	1,380	1,233	1,383	1,326	1,256
Gully density(km/km^2)	0.36	0.3	0.89	1.94	2.14	2.35
Mean slope (degrees)	1.97	6.67	14.1	22.3	24.5	25.7

2.2 Error Estimator and Error Indicator

The true error is not available generally during the computation, so an error estimator is needed. Error estimators do not only provide the means for adaptive optimization of the grid, but are also important for an assessment of the reliability of the results. It is very

desirable to provide for reliable and computationally inexpensive error estimates. Such estimates need to be available for various physically important norms in order to be broadly usable. Miel (1977) proposed a stopping inequality with constant α for new applications of a posteriori error estimates. Babuska and Rheinboldt (1978, 1981) developed a mathematical theory for a class of a posteriori error estimates. Kelly et al. (1983) found that one of the main features of these a-posteriori-error estimates was that they involve local, rather than global, computations. They were given in an asymptotic form which guaranteed accuracy when linked to adaptive refinement algorithms. However, a difficulty was that these error estimates were historically related to adaptive grid schemes so that the asymptotic character of the error estimates was accounted for. De et al. (1983) proposed an error indication and an error estimation, which provided information about where to refine a given grid and when to stop the adaptive process respectively. A value that indicates which grid cells have the larger error, without necessarily telling what the error is, is referred to as an error indicator (Mitchell 1989). Error indication is closely related to the terrain characteristics (Carlisle 2005, Ehlschlaeger and Shortridge 1997, Fisher 1998, Hunter and Goodchild 1997, Kyriakidis et al. 1999, Schneider 2001, Theobald 1989, Wood 1994, Yue 2010, Yue et al. 2007). Loehner (1987) suggested that the error indicator: (1) should be dimensionless so that several key variables can be monitored at the same time; (2) should be bounded so that no further user intervention becomes necessary as the solution evolves; (3) should not only mark the regions with strong shocks to be refined, but also weak shocks, contact discontinuities and other "weak features" in the flow; and (4) should be fast.

For an application of HASM-AM in Dong-Zhi tableland, the error estimator is formulated as,

$$RMSE = \sqrt{\frac{1}{6692}\sum_{l=1}^{6692}(f_l - Sf_l)^2} \tag{11}$$

where *RMSE* is Root Mean-Square Error; f_l is the sampled height on high accuracy at the lth sampled point, $l = 1,2, \ldots ,6692$. Sf_l is the simulated value of $f(x,y)$ in terms of data transformed from contour lines at the lth sampled point.

Simulation results of Dong-Zhi tableland demonstrate that *RMSE* in all landform types of loess plateau becomes larger as grid cell size increases and *RSME* has a close linear relation with grid cell size.

For relatively flat area,

$$RMSE = 2.622 + 0.099h,\ R^2 = 0.947 \tag{12}$$

where h is grid cell size, R is correlation coefficient between h and *RMSE*.

For eroded tableland,

$$RMSE = 5.825 + 0.142h,\ R^2 = 0.963 \tag{13}$$

For loess terrace,

$$RMSE = 3.085 + 0.34h,\ R^2 = 0.994 \tag{14}$$

For loess ridge,

$$RMSE = 6.601 + 0.342h,\ R^2 = 0.990 \tag{15}$$

For loess hill,

$$RMSE = 7.785 + 0.375h, R^2 = 0.977 \tag{16}$$

For loess gully,

$$RMSE = 9.157 + 0.397h, R^2 = 0.975 \tag{17}$$

In general,

$$RSME = a + b \cdot h \tag{18}$$

where a and b are determined by gully density, GD.

According to statistical analyis of data from the Dongzhi tableland, a and b are expressed as the following linear regression equations,

$$a = 3.068 + 0.472 \cdot GD + 0.830 \cdot GD^2, R^2 = 0.807 \tag{19}$$

$$b = -0.038 + 0.416 \cdot GD - 0.103 \cdot GD^2, R^2 = 0.818 \tag{20}$$

In terms of these careful analyses of the requested topographic information, the optimal-grid criterion can be formulated as,

$$RMSE = 3.068 + 0.472 \cdot GD + 0.830 \cdot GD^2 + (-0.038 + 0.416 \cdot GD - 0.103 \cdot GD^2)h \tag{21}$$

The gully density in Dong-Zhi tableland is 0.79 km/km^2. It is required that absolute error is not allowed to be bigger than 40 m. Then, the spatial resolution of DEM should not be coarser than 160 $m \times 160$ m in terms of equation (21). Thus, the starting grid-cell size (or spatial resolution) is selected as 160 $m \times 160$ m for the whole region of Dong-Zhi tableland.

The absolute error is formulated as,

$$AE_l = |f_l - Sf_l| \tag{22}$$

where f_l is the sampled height at the kth sampled point, Sf_l is the simulated value of $f(x,y)$ at the lth sampled point; $l = 1,2, \ldots, 6692$.

Then, an error surface can be interpolated in terms of the absolute error calculated at every sampled point under combination with equations (12), (13), (14), (15), (16) and (17). The location of the sampled point determines which equation is used to interpolate the error surface around the sampled point.

The error indicator is defined as

$$EI_{i,j} = \frac{AE_{i,j}}{40} \tag{23}$$

where $EI_{i,j}$ is the error indicator at lattice (i,j); $AE_{i,j}$ is the interpolated absolute error at lattice (i,j), $i = 1,2, \ldots, I$, $j = 1,2, \ldots, J$.

2.3 Adaptive Refinement

For HASM-AM, grid cells on which $EI_{i,j} > 1$ get into the refinement process. The refinement process is stopped for grid cells where $EI_{i,j} \leq 1$. The method to refine the grid includes six steps as follows:

1. The whole domain is simulated on the optimal-grid cell size (or spatial resolution) of $h \times h$ for starting by operating HASM, $A_h U^{n+1} = B_h^n$, and the simulated values are obtained on the spatial resolution of $h \times h$, in which $h = 160\ m$.
2. $AE_{i,j}(i = 1,2, \ldots, I; j = 1,2, \ldots, J)$ on every grid cell (i,j) is interpolated by combining the calculated absolute errors at the sampled points with equations (11) through (17) under consideration of landforms. If $EI_{i,j} > 1$, the grid cell (i,j) is flagged for refinement.
3. The flagged grid cells are clustered into different refinement sub-domains, $SD_{1,1}$, $SD_{1,2}, \ldots, SD_{1,K}$, where K is the number of sub-domains to be refined.
4. Every grid cell in the sub-domains, $SD_{1,1}, SD_{1,2}, \ldots, SD_{1,K}$, is bisected by connecting the midpoints of two sides with their opposite sides, which forms four smaller grid cells of equal areas with a spatial resolution of $\frac{h}{2} \times \frac{h}{2}$.
5. The information on coarser grid cells is transferred to the finer grid cells.
6. The equations of HASM, $A_{\frac{h}{2}} U^{n+1} = B_{\frac{h}{2}}^n$, are solved respectively in the sub-domains, $SD_{1,1}, SD_{1,2}, \ldots, SD_{1,K}$.
7. The process from step ② (2) to step ⑥ (6) is repeated until all grid cells meet the requirement for accuracy.

The error distribution map (Figure 2a) shows that simulation error is closely related to gully density. The higher the gully density, the bigger the error. All grid cells in flat area satisfy $EI_{i,j} \leq 1$. Error analysis demonstrates that the first simulation has a maximum error of 224.7 m, mean error of 43.2 m, and standard deviation of 33.0 m. The number of grid cells where $EI_{i,j} > 1$ accounts for 30% of the surface.

The grid cells where $EI_{i,j} > 1$ are bisected and then simulated on spatial resolution of 80 m × 80 m secondly. The error calculation (Figure 2b) demonstrated that grid cells of $EI_{i,j} > 1$ account for 24% of the grid cells after the second simulation. The maximum error decreases to 149.4 m, mean error to 27.3 m, and standard deviation to 20.1 m.

For the 24% of the grid cells where $EI_{i,j} > 1$, refinement is conducted once again and then simulation is implemented at a spatial resolution of $40\ m \times 40\ m$. After the third simulation, 3% of grid cells on which $EI_{i,j} > 1$ remain. The maximum error is 99.4 m; mean error is 15.1 m; and standard deviation is 10.8 m (see Figure 2c).

The 3% of grid cells on which $EI_{i,j} > 1$ are thirdly bisected into finer grid cells at a spatial resolution of 20 m × 20 m. According to the error distribution map (see Figure 2d), grid cells of $EI_{i,j} > 1$ only account for 0.1% of the grid cells. The maximum error decreases to 64.3 m, mean error to 10.7 m and standard deviation to 6.7 m.

The remaining grid cells on which $EI_{i,j} > 1$ are refined fourthly. According to the error distribution map of the fifth simulation conducted at a spatial resolution of 10 m × 10 m (Figure 2e), all grid cells satisfy $EI_{i,j} \leq 1$. The final maximum error is 40 m, mean error is 8.5 m and standard deviation is 5.3 m. The final elevation surface of the Dong-Zhi tableland is obtained after the refinement process has been finished (Figure 3 and Table 2).

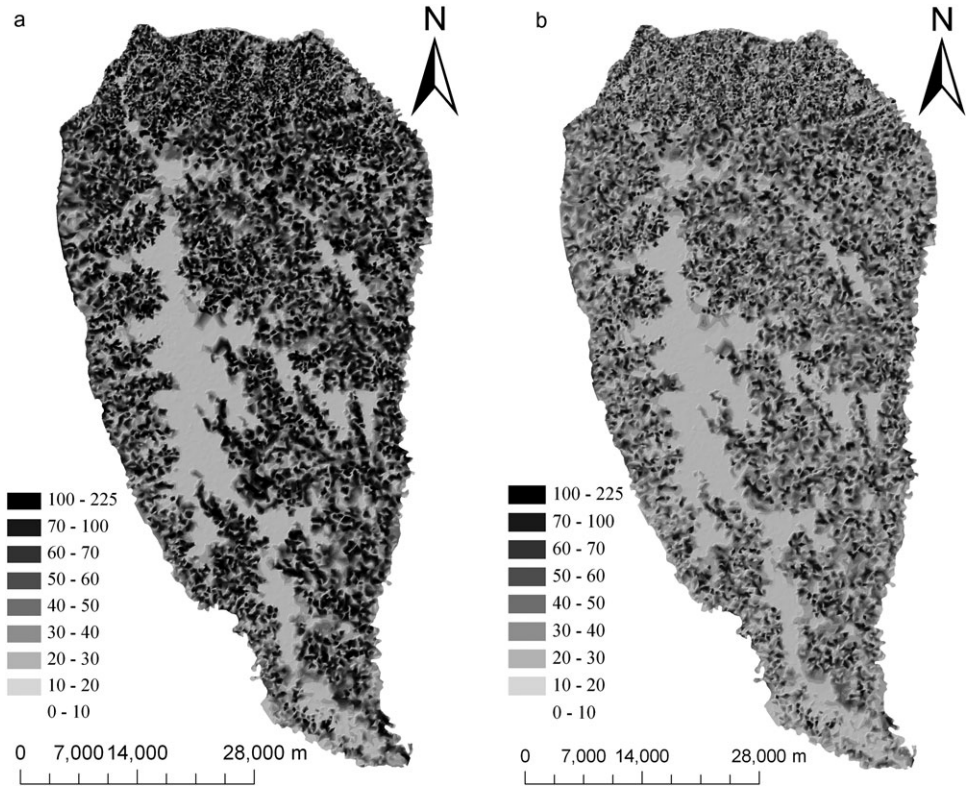

Figure 2 Error distribution map: (a) the first simulated Dongzhi tableland on a spatial resolution of 160 m × 160 m; (b) the second simulated Dong-Zhi tableland after the first local refinement on a spatial resolution of 80 m × 80 m; (c) the third simulated Dong-Zhi tableland after the second local refinement on a spatial resolution of 40 m × 40 m; (d) the fourth simulated Dong-Zhi tableland after the third local refinement on a spatial resolution of 20 m × 20 m; and (e) the fifth simulated Dong-Zhi tableland after the fourth local refinement on a spatial resolution of 10 m × 10 m

2.4 Test of Computational Efficiency

If the elevation surface of the Dong-Zhi tableland were to be simulated by HASM, 27.24 million of grid cells would be calculated on the spatial resolution of 10 $m \times 10$ m, while HASM-AM only deals with about 870,000 grid cells, such that the computational efficiency is greatly improved.

As the whole of the Dong-Zhi tableland is too big to be simulated at the spatial resolution of 10 $m \times 10$ m for classic methods such as inverse distance weighting (IDW) (Shepard 1968), Kriging (Krige 1951) and Splines (Watt 2000). A region with an area of 26.5 km^2 is selected to analyze comparatively the computation time of HASM-AM. In this region, the standard deviation of elevation is 53.5 m. It is located from 35°49′59″ to 35°52′30″N and from 107°33′45″ to 107°37′30″E, where the maximum elevation and minimum elevation are 1,450 and 1,225 m, respectively (Figure 4).

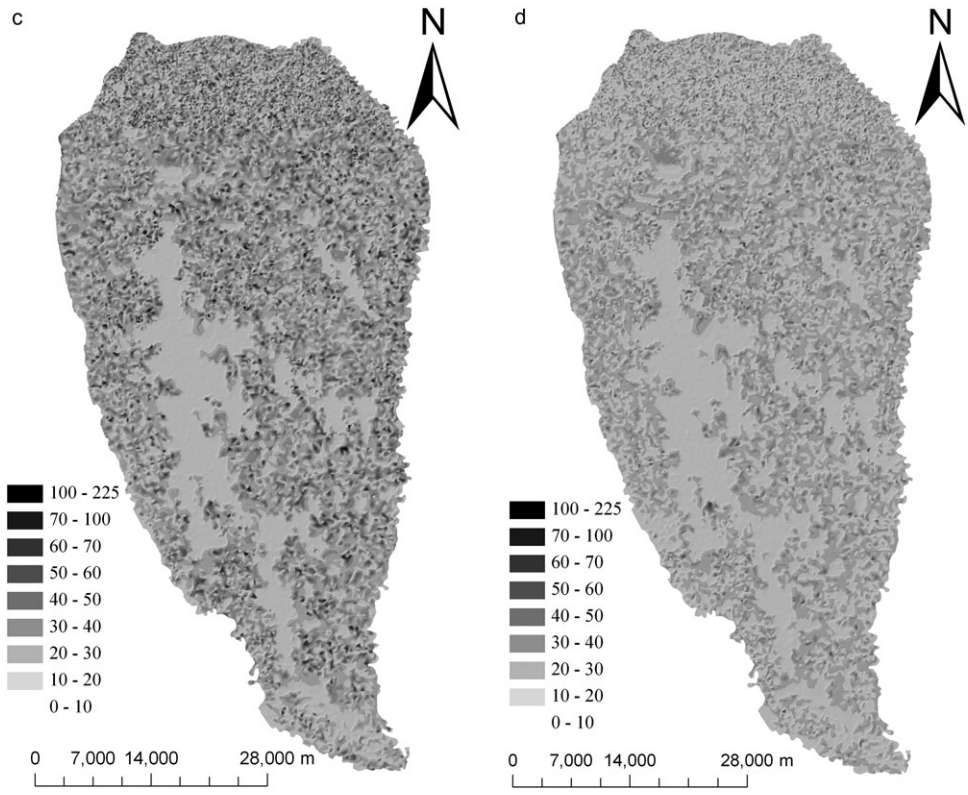

Figure 2 Continued

The simulated elevation surface consists of 265,000 grid cells on a spatial resolution of 10 m × 10 m. The test results (Table 3) show that HASM-AM has the highest accuracy and the fastest computation speed, compared with HASM, IDW, Splines and Kriging. HASM-AM created a surface with an RMSE of 11.1 m and accomplished the simulation process in 10.9 s. The RMSE and computing time of HASM are 11.5 m and 19.2 s, respectively. It means that the introduction of the adaptive method improved both computational speed and simulation accuracy. Kriging, IDW and Splines spent 2,807, 449 and 438 s to accomplish their simulation processes and created surfaces with RMSEs of 12.3, 12.2 and 31.5 m, respectively. Both HASM-AM and HASM have much higher computational speed and accuracy than the classic methods.

3 Discussion and Conclusions

Defining a global grid for the discretization of a given problem independently of the solution process is often insufficient. The adaptivity of grids is one of the major trends in numerical simulation and scientific computing. In the adaptive multigrid process finer and finer grids are not constructed globally. They are only constructed in

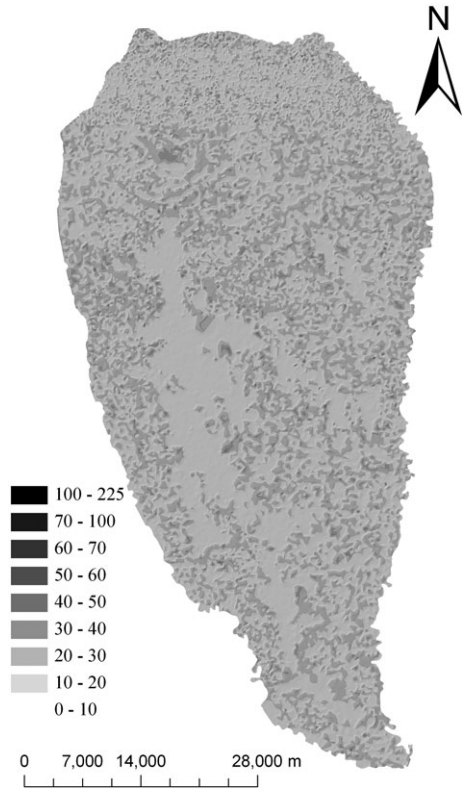

Figure 2 Continued

those parts of the domain where the current discretization error is significantly large. An adaptive simulation approach with grid selection strategies is highly significant for HASM, which is a very desirable feature for an accurate analysis and an efficient simulation. The adaptive approach can be distinguished into predefined refinement and self-adaptive refinement. In predefined refinement, the refinement is determined before the solution process is started; in self-adaptive approaches, the grid refinements are carried out dynamically during the solution process (Trottenberg et al. 2001). In the process of simulating the elevation surface of the Dong-Zhi tableland, the predefined refinement and self-adaptive refinement are combined.

Adaptivity can help to resolve local scales that interact with global scales in a consistent way (Behrens 2006). The most demanding difficulty for adaptive methods is to find a suitable refinement criterion. An adaptive method is only as good as the refinement criterion that controls adaptivity. Thus, a good understanding is needed for what accuracy really means in the context of the problem and full insight into the reason for error is required if one aims at substantial improvement in the accuracy of the solution. An effective refinement criterion needs to detect those areas that cause the highest error or that are of the highest interest, concerning the relevant physical features. It is found that gully density and grid cell size define the effective refinement criterion in the case of the Dong-Zhi tableland.

HASM-AM helps to speed up the computation of HASM by avoiding unnecessary calculations and saving memory. The test result shows that the introduction of the

Figure 3 Shaded relief map in 3D of Dong-Zhi tableland simulated after the refinement process is stopped (Light from 135° with a dip angle of 45°)

Table 2 Improving accuracy of simulation process by adaptive refinement

Simulation process	Maximum error (m)	Mean error (m)	Standard deviation (m)	Percentage of grid cells with $EI > 1$ (%)
First simulation of the whole domain	224.7	43.2	33.0	30
Second simulation after the first refinement	149.4	27.3	20.1	24
Third simulation after the second refinement	99.4	15.1	10.8	3
Fourth simulation after the third refinement	64.3	10.7	6.7	0.1
Fifth simulation after the fourth refinement	40	8.5	5.3	0

Table 3 Comparisons of computing time and simulation accuracy

Method	Time (seconds)	RMSE (m)
Kriging	2,807	12.3
IDW	449	12.2
Spline	438	31.5
HASM	19.2	11.5
HASM-AM	10.9	11.1

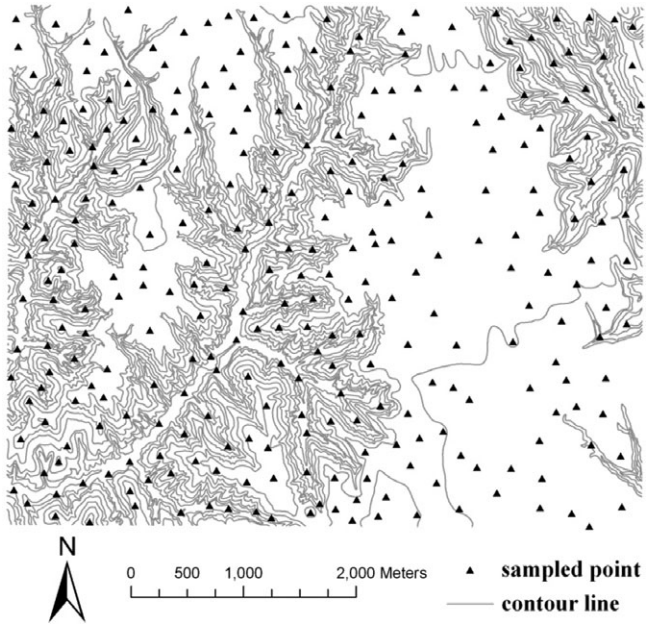

Figure 4 The sector map on a spatial scale of 1/10,000 of the test area, in which curves are contour lines and black triangles are sampled heights of high accuracy

adaptive method shortens computation time of HASM from 19.2 s to 10.9 s. The computational speed of HASM-AM increases by 43.2% compared with HASM. HASM-AM is 256, 40 and 39 times faster than the classical methods, Kriging, IDW and Spline, respectively. In addition, HASM-AM has the highest accuracy.

The adaptive refinement technique is very successful in reducing the computational and storage requirements for solving the partial differential equations of HASM. The adaptive refinement technique places more grid cells in areas where the local error in the solution is large instead of using a uniform mesh with grid cells evenly spaced on a domain. If a non-uniform grid is generated by an adaptive refinement algorithm and portioned into a number of sets equal to the number of processors, a parallel algorithm for the adaptive refinement can be developed, which would much greatly speed up the computation of HASM-AM. Our next effort will be to create this HASM-AM parallelization.

Acknowledgments

This work is supported by the China National Science Fund for Distinguished Young Scholars (40825003), the National High-tech R&D Program of the Ministry of Science and Technology of the People's Republic of China (2006AA12Z219), and by the National Key Technologies R&D Program of Ministry of Science and Technology of the People's Republic of China (2006BAC08). This research was also partially supported by U.S. National Science Foundation's Biocomplexity and LTER Programs and the University of California Agricultural Experiment Station.

References

Atkinson P M 2002 Surface modelling: What's the point? *Transactions in GIS* 6: 1–4

Babuska I and Rheinboldt W 1978 Error estimates for adaptive finite element computations. *SIAM Journal on Numerical Analysis* 15: 736–54

Babuska I and Rheinboldt W 1981 A posteriori error analysis of finite element solutions for one-dimensional problems. *SIAM Journal on Numerical Analysis* 18: 565–89

Behrens J 2006 *Adaptive Atmospheric Modelling*. Berlin, Springer-Verlag

Birchfield G E 1960 Numerical prediction of hurricane movement with the use of a fine grid. *Journal of Meteorology* 17: 404–14

Brandt A 1977 Multilevel adaptive solutions to boundary value problems. *Mathematics of Computation* 31: 333–90

Carlisle B H 2005 Modelling the spatial distribution of DEM error. *Transactions in GIS* 9: 521–40

De J P, Gago S R, Kelly D W, Zienkiewicz O C, and Babuska I 1983 A posteriori error analysis and adaptive processes in the finite element method: Part II, Adaptive mesh refinement. *International Journal for Numerical Methods in Engineering* 19: 1621–56

Ehlschlaeger C R and Shortridge A 1997 Modelling elevation uncertainty in geographical analyses. In Kraak M J and Molenaar M (eds) *Advances in GIS Research: Proceedings of the Seventh International Symposium on Spatial Data Handling*. London, Taylor and Francis: 585–95

Evans I S 1980 An integrated system of terrain analysis and slope mapping. *Zeitschrift fuer Geomorphologie* Suppl-Bd 36: 274–95

Fisher P 1998 Improved modelling of elevation error with geostatistics. *GeoInformatica* 2: 215–33

Harrison E J Jr 1973 Three-dimensional numerical simulations of tropical systems utilizing nested finite grids. *Journal of the Atmospheric Sciences* 30: 1528–43

Huang Z and Lees B 2005 Representing and reducing error in natural-resource classification using model combination. *International Journal of Geographical Information Science* 19: 603–21

Hunter G J and Goodchild M F 1997 Modeling the uncertainty of slope and aspect estimates derived from spatial databases. *Geographical Analysis* 29: 35–49

Kelly D W, De J P, Gago S R, Zienkiewicz O C, and Babuska I 1983 A posteriori error analysis and adaptive processes in the finite element method: Part I – error analysis. *International Journal for Numerical Methods in Engineering* 19: 1621–56

Kidner D B, Ware J M, Sparkes A J, and Jones C B 2000 Multiscale terrain and topographic modelling with the implicit TIN. *Transactions in GIS* 4: 379–408

Krige D G 1951 A Statistical Approach to Some Mine Valuations and Allied Problems at the Witwatersrand. Unpublished M.S. Thesis, University of Witwatersrand

Kyriakidis P C, Shortridge A M, and Goodchild M F 1999 Geostatistics for conflation and accuracy assessment of digital elevation models. *International Journal of Geographical Information Science* 13: 677–707

Leigh C L, Kidner D B, and Thomas M C 2009 The use of LiDAR in digital surface modeling: Issues and errors. *Transactions in GIS* 13: 345–61

Ley G W and Elsberry R L 1976 Forecasts of typhoon Irma using a nested-grid model. *Monthly Weather Review* 104: 1154–61

Loehner R 1987 An adaptive finite element scheme for transient problems in CFD. *Computer Methods in Applied Mechanics and Engineering* 61: 323–38

Miel G 1977 On a posteriori error estimates. *Mathematics of Computation* 31(137): 204–13
Mitchell W F 1989 A comparison of adaptive refinement techniques for elliptic problems. *ACM Transactions on Mathematical Software* 15: 326–47
Morrison D 1962 Optimal mesh size in the numerical integration of an ordinary different equation. *Journal of the Association for Computing Machinery* 9: 98–103
Okubo T 1987 *Differential Geometry*. New York, M. Dekke
Schmidt A and Siebert K G 2005 *Design of Adaptive Finite Element Software*. Berlin, Springer-Verlag
Schneider B 2001 Phenomenon-based specification of the digital representation of terrain surfaces. *Transactions in GIS* 5: 39–52
Shepard D 1968 A two-dimensional interpolation function for irregularly-spaced data. *Proceedings of the Twenty-third ACM National Conference*. Cleveland, Ohio: 517–24
Theobald D M 1989 Accuracy and bias issues in surface representation. In Goodchild M F and Gopal S (eds) *The Accuracy of Spatial Databases*. London, Taylor and Francis: 99–106
Toponogov V A 2006 *Differential Geometry of Curves and Surfaces*. New York, Birkhaeuser
Trottenberg U, Oosterlee C W, and Schueller A 2001 *Multigrid*. London, Academic Press
Unwin D J 1995 Geographical information systems and the problems of "error and uncertainty". *Progress in Human Geography* 19: 549–58
Watt A 2000 *3D Computer Graphics*. New York, Addison-Wesley
Wood J D 1994 Visualising contour interpolation accuracy in digital elevation models. In Hearnshaw H M and Unwin D J (eds) *Visualization in Geographical Information Systems*. Chichester, John Wiley and Sons: 168–80
Yue T X 2010 *Surface Modelling: High Accuracy and High Speed Methods*. Boca Raton, FL, CRC Press
Yue T X and Ai N S 1990 A morphological mathematical model for cirques. *Glaciology and Cryopedology* 12: 227–34 (in Chinese)
Yue T X and Song Y J 2008 The YUE-HASM Method. In Li D, Ge Y, and Foody G M (eds) *Accuracy in Geomatics*. Liverpool, World Academic Union: 148–53
Yue T X, Chen S P, Xu B, Liu Q S, Li H G, Liu G H, and Ye Q H 2002 A curve-theorem based approach for change detection and its application to Yellow River delta. *International Journal of Remote Sensing* 23: 2283–92
Yue T X, Wang Y A, Chen S P, Liu J Y, Qiu D S, Deng X Z, Liu M L, and Tian Y Z 2003 Numerical simulation of population distribution in China. *Population and Environment* 25: 141–63
Yue T X, Fan Z M, and Liu J Y 2005 Changes of major terrestrial ecosystems in China Since 1960. *Global and Planetary Change* 48: 287–302
Yue T X, Fan Z M, Liu J Y, and Wei B X 2006 Scenarios of major terrestrial ecosystems in China. *Ecological Modelling* 199: 363–76
Yue T X, Du Z P, Song D J, and Gong Y 2007 A new method of surface modeling and its application to DEM construction. *Geomorphology* 91: 161–72
Yue T X, Du Z P, and Song Y J 2008 Ecological models: Spatial models and geographic information systems. In Jørgensen S E and Fath B (eds) *Encyclopedia of Ecology*. England, Elsevier: 3315–25
Zhou Q M and Liu X J 2002 Error assessment of grid-based flow routing algorithms used in hydrological models. *International Journal of Geographical Information Science* 16: 819–42